ChemComm

COMMUNICATION

Ambipolar macrocycle derived from spiro-xanthene and carbazole: synthesis, structure–property relationships, electronic properties and host–guest investigation†
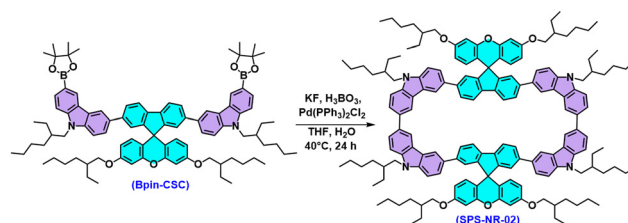
Phani Kumar Kodali, [ID] [ab] Sairathna Choppella, [ID] [c] Ankita, [d] Deepak Kumar, [ab] Upendra Kumar Pandey, [ID] [d] Mahesh Kumar Ravva [ID] [c] and Surya Prakash Singh [ID] *[a]

For the first time, we present the detailed synthesis, photophysical, electrochemical, host–guest and charge transport properties of spiro[fluorene-9,9′-xanthene] (SFX) and carbazole macrocycle SPS-NR-02. The electron and hole transport values measured using the space charge limited current (SCLC) method resulted in ambipolar charge transport with an electron to hole mobility ratio of 0.39.

Macrocyclic conjugated systems such as cyclacenes, cyclophencens and cyclo-oligophenylenes are an intriguing class of molecules because of their infinite cyclic conjugation, well-defined diameters and delocalized electronic structures.[1–3] When compared to their linear analogues (oligo *para*-phenylenes), these strained macrocyclic molecules display contrasting properties like decreasing band gap with a reduction in the size of the ring,[4] red-shift in emission as the size of the hoop decreases,[5] increase in their relative solubility and the ability to use the void to accommodate electronically important guest molecules like fullerene.[6] In particular, macrocycles have potential applications in organic electronics.[7] Similar to linear conjugated molecules, the choice of donor and acceptor moieties defines the electronic and optical properties of macrocyclic compounds as they modulate the energy levels of the molecules.[8] Utilizing this strategy, different donor–acceptor macrocycles have been reported and demonstrated their applications in organic solar cells (OSCs), organic light emitting diodes (OLEDs) and organic field effect transistors (OFETs).[9] Along with this, it was proven by Jasti and co-workers that important photophysical properties of cyclic compounds can be altered by changing the connectivity of carbon atoms,

size and symmetry.[10] Owing to these advantages, these stained macrocycles performed better than their linear analogues when deployed as an active layer in organic electronic devices.[11] Hence, it is essential to synthesize macrocycles with different acceptor and donor moieties to establish precise structure–property relationships and to eventually enhance their performance in organic electronic devices. Linear donor–acceptor molecules with an SFX core have been successfully deployed as hole transporting materials and thermally activated fluorescence emitters for perovskite solar cell and OLED applications, respectively, with excellent efficiencies because of their unique properties like non-dispersive hole transporting ability and ambipolar charge transporting properties.[12] Cyclic carbazoles were extensively studied by Poriel and co-workers to understand the effects of *N*-bridging on cyclo-*para* phenylenes and were used in OFET and OLED applications.[11,13] As part of this communication, we report the synthesis, photophysical, electrochemical and ambipolar charge transport properties of SFX and carbazole incorporated macrocycle SPS-NR-02.

The macrocycle presented in this work is synthesized (Scheme 1) following the oxidative homocoupling of aryl boronic esters methodology developed by Jasti and co-workers.[14] To begin with, the SFX core was synthesized using a condensation reaction between 2,7-dibromofluorenone and resorcinol. The synthesized SFX core was *O*-alkylated using 2-ethylhexyl alkyl chains to overcome the solubility issues that would arise in the next steps. The all-important boronic ester precursor for macrocycle synthesis Bpin-CSC was achieved by a series of Suzuki coupling and Suzuki–

[a] Department of Polymers and Functional Materials, CSIR-Indian Institute of Chemical Technology (IICT), Uppal Road, Tarnaka, Hyderabad 500007, India. E-mail: spsingh@iict.res.in

[b] Academy of Scientific and Innovative Research (AcSIR), Ghaziabad-201002, India

[c] Department of Chemistry, SRM University-AP, Amaravati 522240, India

[d] Department of Electrical Engineering, School of Engineering, Shiv Nadar Institution of Eminence, Delhi NCR, 201314, India

† Electronic supplementary information (ESI) available: Synthesis, spectroscopy, electrochemistry, molecular modelling, and NMR. See DOI: https://doi.org/10.1039/d4cc03440f

Scheme 1 Synthesis of macrocycle SPS-NR-02.

Miyaura borylation reactions. Finally, oxidative homocoupling of the borylated precursor provided the final macrocycle SPS-NR-02 with 18% yield. The detailed synthetic route is shown in Scheme S1 (ESI†). The MALDI-TOF mass spectrum of SPS-NR-02 showed an experimental molecular weight of 2282.42 Da (calculated 2282.424 Da, Fig. S37, ESI†). The experimental isotopic distribution of the mass peak of the final molecule fits the chemical formula of SPS-NR-02 and matches well with the theoretical simulation, as shown in Fig. S38 (ESI†). Although the number of hydrogen atoms revealed by the integration of ^{1}H NMR of SPS-NR-02 matches the chemical formula, the NMR peaks in the aromatic region cannot be assigned precisely due to the overlapping NMR signals (Fig. S27, ESI†). We did not observe the clear splitting of NMR signals even after recording ^{1}H NMR at 273.15 K (Fig. S29, ESI†). We did not observe the formation of macrocycles of the sizes other than the one mentioned in the procedure.[10,13b,15] Even after numerous efforts with different crystallization conditions and solvents, we were unsuccessful in obtaining a single crystal of the synthesized molecule to understand the molecular geometry. This could be because of the branched 2-ethylhexyl alkyl chains which hinder the formation of crystal growth.[9a,13a] Thus, DFT calculations have been conducted to gain insights into the geometrical and photophysical properties of SPS-NR-02. The 2-ethylhexyl alkyl chains have been replaced by methyl groups to simplify DFT calculations. The conformational stability is further elucidated by analysing the molecular strain arising from the orientation of the xanthene group relative to the molecular backbone.[16] The molecules were optimized to their minimum energy structure at the ωB97XD/6-31G(d,p) level of theory. All calculations are performed using the Gaussian16 package. The optimized geometries of various SPS-NR-02 macrocycle conformations are illustrated in Fig. 1. Among these, conformations where the molecules with spiro-linkage are in opposite planes are labelled as 'A.' While those in which the spiro linkage is on the same plane are labelled as 'B.' While considering the role of spiro linkage, the strain analysis (Fig. S8 and Table S9, ESI†) shows a slight increase in strain energy in SPS-NR-02-B (5.67 kcal mol^{-1}) compared to SPS-NR-02-A (2.05 kcal mol^{-1}), where the orientation of the substituents with higher steric hindrance contributes to reduced stability. The geometry of SPS-NR-02 is not perfectly circular, with a dihedral angle of 43° between carbazole and fluorene units (Fig. S11, ESI†), creating a rectangular hoop. The C–C bond lengths of carbazole are all equal (∼1.39 nm), indicating the benzenoid character of carbazole.
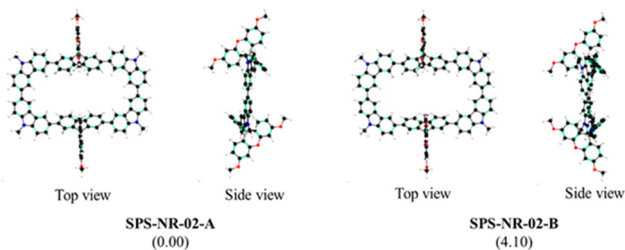
The relative energies and strain energy calculations conclude that the conformation SPS-NR-02-A is the most favorable conformation. In further discussions, SPS-NR-02-A is referred to as SPS-NR-02.

The absorption and emission spectrum of SPS-NR-02 displayed two structured bands at 309 nm and 351 nm (absorption) and 397 nm and 416 nm (emission), respectively, and is shown in Fig. 2. The absorption coefficient (ε) of SPS-NR-02 at the absorbance maxima was $\varepsilon = 1.26 \times 10^5$ M^{-1} cm^{-1} (Fig. S1 and Tables S1, S2, ESI†). Next, the absorption and emission properties were recorded in solvents of increasing polarity. With an increase in the solvent polarity, the absorption maxima slightly red-shifted by 8 nm, while the absorption peak at 309 nm remains unaffected (Fig. S2a, ESI†). In the case of fluorescence spectra, we observed a bathochromic shift of the emission maxima by 34 nm from λ_{ems}-387 nm (cyclohexane) to λ_{ems}-421 nm (DCM) (Fig. 2), with the emission spectra becoming broadened and structure-less. Fluorescence spectroscopy recorded in toluene resulted in deep-blue emission with CIE coordinates CIE$_{[x,y]}$ = [0.16,0.041] (Fig. S3, ESI†). The linear plot between the wavenumber of emission in different solvents versus solvent parameter $E_T(30)$ (Fig. S2b and Table S3, ESI†) indicates positive solvatochromism, which is in turn because of the donor–acceptor nature of SPS-NR-02. Absolute quantum yield was recorded on an Edinburgh FLS1000 instrument using the integrating sphere accessory showing a photoluminescence quantum yield (PLQY) in the range 14% (cyclohexane) to 53% (toluene).

The nature of the first ten excited states of SPS-NR-02 was investigated using TD-DFT, the screened range-separated hybrid functional (SRSH) LC-ωHPBE/6-31G(d,p) method and natural transition orbital analysis (NTO) in the presence of the PCM solvent model (Fig. S9 and Table S11, ESI†).[17] In the case of SPS-NR-02, the first excitation and emission are forbidden with zero oscillatory strength. The second excitation, characterized by the maximum oscillatory strength ($f = 2.76$), shows absorption at 350 nm. This excitation arises from the combined contributions of two particle–hole pairs. Similarly, from theoretical studies, the second, less intense peak at 310 nm ($f = 0.43$) corresponds to the second absorption peak from experimental absorption spectra. In this case, one pair of NTOs, with half of the weightage, demonstrates HLCT character, whereas the other pair shows a clear charge-transfer state corresponding to a transition from carbazole units to fluorene units. The two peaks in the emission spectra at 397 nm and 416 nm represent the second and third excited states from theoretical calculations. In this context, the excitation corresponding to the peak at 397 nm exhibits HLCT character. In comparison, the peak at 416 nm corresponds to a charge transfer from carbazoles to SFX.
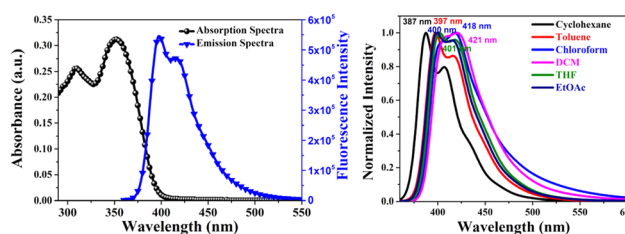

Fig. 1 Optimized geometries of possible conformations of SPS-NR-02 obtained at the ωB97XD/6-31G(d,p) level of theory. The relative energies are given in kcal mol^{-1}.

Fig. 2 UV-vis and fluorescence spectra of SP-NR-2 (left). Emission spectra in solvents of increasing polarity (right).

The bi-exponential fitting of time-resolved photoluminescence (TRPL) decays indicates the involvement of two different components during emission (Fig. S4 and Table S5, ESI†). The average fluorescence lifetime τ_{avg} of SPS-NR-02 is in the range of 1.382 ns to 1.733 ns for all the solvents except for cyclohexane (τ_{avg} is 2.396 ns) denoting similar deactivation pathways. The fast component τ_1 varies between 0.88 ns and 1.126 ns with 77.9% to 95.2% relative contribution and the slow component τ_2 varies between 2.587 ns to 3.768 ns with relative contributions ranging from 4.68% to 22.08% in various solvents. In the case of toluene solvent, the value of the radiative rate constant (k_r = 0.309 ns^{-1}) is higher than the value of the non-radiative rate constant (k_{nr} = 0.2677 ns^{-1}) and when it comes to cyclohexane solvent, the value of k_{nr} (0.357 ns^{-1}) is six folds higher than k_r (0.0601 ns^{-1}). This could be the reason for the lower PLQY in cyclohexane solvent when compared with toluene solvent. As indicated in the previous paragraph, the excited states have HLCT characters and as a result, SPS-NR-02 shows both solvatochromism and decent quantum yields.[18]

The cyclic voltammogram (CV) of SPS-NR-02 (100 mM) shows one reversible and one quasi-reversible oxidation process with maxima at 0.89 V and 1.05 V (versus Fc/Fc$^+$), respectively, and one irreversible and one quasi-reversible reduction process with maxima at −0.96 V and −1.32 V (versus Fc/Fc$^+$) (Fig. 3 and Fig. S6, ESI†). HOMO and LUMO values calculated from the onset potentials of the first oxidation (E_{onset}^{oxd} = 0.77 eV) and reduction waves (E_{onset}^{oxd} = −0.7 eV) are −5.17 eV and −3.7 eV (Table S7, ESI†). Experimental HOMO (−5.17 eV) values are in correlation with the theoretical data (−5.32 eV). The calculated electrochemical band gap is about 1.47 eV. As revealed by DFT analysis, the HOMO wavefunction is delocalized throughout the ring and the LUMO is localized on the acceptor units (Fig. S10, ESI†). When we consider individual moieties of donor (carbazole) and acceptor (SFX group), the HOMO energy of carbazole is −5.80 eV and the LUMO energy of the SFX group is −0.63 eV. While after the formation of a macrocycle, the HOMO is well destabilized but the LUMO is slightly stabilized. This suggests a moderate donor and acceptor nature between carbazole and the SFX unit in the macrocycle (Table S8, ESI†). We have also calculated the amount of net charge transfer ($|e|$) between the donor and acceptor groups in the macrocycle in the ground and excited states. The amount of charge transferred from donor to acceptor is negligible in the ground state and most of the excited states, and in some excited states, it is minimum (≤ 0.5). Along with that, we have

observed a relatively low $\Delta\mu$ (difference between excited and ground state dipole moments) between the ground and excited states. These observations indicate the donor–acceptor character of the macrocycle (Tables S10 and S11, ESI†). From NTOs, we can observe that, the electron population is more localized on the SFX units, whereas the hole is either completely distributed on the backbone or localized on the carbazole units in SPS-NR-02. This confirms the donor and acceptor nature of SPS-NR-02 in some of the excited states.

The unique characteristics of macrocycles lie in their ability to accommodate guest molecules due to their cyclic structure. Upon examining the distances between the SFX unit centroids (9.89 nm) and carbazole unit centroids (14.23 nm) in the macrocycle, it becomes evident that it can accommodate C_{60} (Fig. S15, ESI†). These dimensions are substantial, making it feasible for the macrocycle to host molecules such as C_{60}. The fluorescence titration of SPS-NR-02 against increasing concentrations of C_{60} resulted in complete quenching of fluorescence. The binding association constant calculated from the Stern–Volmer equation is K_a = 9.95 × 10^4 M^{-1} (Fig. S12, ESI†). An isosbestic point at 392 nm was observed in the absorption spectra recorded by mixing different ratios of SPS-NR-02 and C_{60} (Fig. S13, ESI†). Furthermore, the calculated counterpoise corrected interaction energy, utilizing the supermolecule approach, is −42.98 kcal mol^{-1}, indicating that the complex is more stable than the individual molecules (Fig. S15, ESI†). Following complexation, the strain energy of SPS-NR-02 increased to 18.8 kcal mol^{-1}, attributed to the strain induced by C_{60}, causing the macrocycle to become more circular (Fig. S16 and Table S12, ESI†). We analysed the nature of the interaction between the macrocycle and C_{60} using symmetry-adapted perturbation theory (SAPT) analysis and found out that the dispersion energy (−105.75 kcal mol^{-1}) is the predominant factor for stabilizing the complex, suggesting that the interaction relies heavily on weak interactions (Table S13, ESI†). CV of SPS-NR-02 recorded after adding equimolar and increasing concentrations of C_{60} remain unchanged (Fig. S14, ESI†). NTO analysis was used to explore the nature of the excitation. Fig. 4 depicts a distinct charge transfer state in the lowest excited state, wherein the hole is localized on a nanohoop and the electron is localized on C_{60}.

Hole and electron mobilities of SPS-NR-02 are determined using SCLC by averaging the five best devices (Table S14, ESI†) and are summarized in Table 1 and Fig. 5. It is important to note that these values of hole and electron mobilities are lower
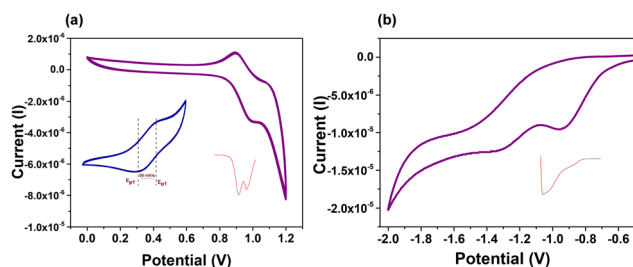

Fig. 3 CV of SPS-NR-02 (100 mM) on (a) oxidation (inset-first oxidation process) and (b) reduction recorded in DCM (n-Bu4NPF6, 0.1 M). Pt working electrode and sweep rate 50 mV s^{-1}. The first derivatives of the voltammograms are shown as red traces.

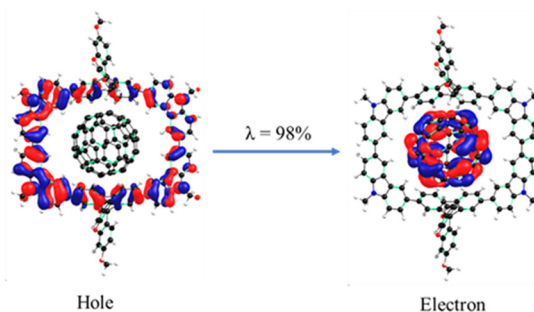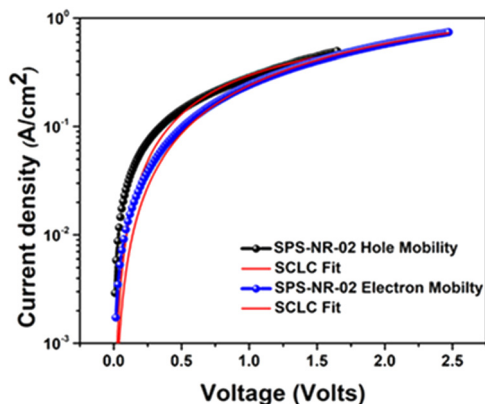**Fig. 4** Hole and electron wavefunction plots of SPS-NR-02/C60 obtained at the SRSH-LC-ωHPBE/6-31G(d,p) level of theory using toluene as a solvent.

Table 1 Summary of hole and electron mobility values measured using the SCLC method

Molecule	Hole mobility (cm^2 V^{-1} s^{-1})	Electron mobility (cm^2 V^{-1} s^{-1})	μ_e/μ_h ratio
SPS-NR-02	$4.75 \pm 0.54 \times 10^{-3}$	$1.87 \pm 0.29 \times 10^{-3}$	0.39

Fig. 5 J–V characteristics in the semi-log plot used to extract hole and electron mobility of SPS-NR-02 using the modified Mott–Gurney space charge limited current technique.

bounds; trapping of charge carriers or non-ohmicity of the injecting electrodes will lead to even higher mobility values. For SPS-NR-02 we observed hole and electron mobility of μ_h = 4.75×10^{-3} cm^2 V^{-1} s^{-1} and μ_e = 1.87×10^{-3} cm^2 V^{-1} s^{-1}, respectively. When compared with the reported charge transport properties of nanohoops, the electron mobility of SPS-NR-02 is significantly higher than the highest electron mobility reported by Du and co-workers[19] (μ_e = 1.8×10^{-4} cm^2 V^{-1} s^{-1}) and hole mobility reported by Poriel and co-workers ($\mu_{carrier}$ = 2.78×10^{-4} cm^2 V^{-1} s^{-1}).[20] Since the macrocycle we reported in this work differs from nanohoops only in terms of connectivity, we feel comparison with nanohoops is judicious, especially in electronics, which highlights the different effects of curvature. This significant increase in hole mobility could be because of the size of the macrocycle, which is in correlation with the work done by Poriel and co-workers who put forward that charge transport properties increase with increase in the size of the ring and also because of the donor–acceptor nature of the macrocycle, as suggested by the theoretical work done by Negri and co-workers who suggested that owing to orbital localization, charge transport for a D–A macrocycle becomes more efficient than [n]cycloparaphenylene.[13b,21] Moreover, this molecular architecture has led to relatively balanced ambipolar charge transport with a μ_e/μ_h ratio of 0.39, which has potential application in single-layer OFET and OLED devices.[22] The ambipolar electron and hole mobilities achieved for SPS-NR-02 suggest that future work is needed to establish better structure–property relations of D–A macrocycles and to design macrocycles with higher charge mobilities, which would eventually help in deploying these macrocyclic scaffolds in organic electronic devices.

In summary, a bridged D–A macrocycle SPS-NR-02 was synthesized by connecting the carbazole and SFX. The macrocycle displayed positive solvatochromism, and DFT analysis revealed delocalized HOMO and localized LUMO. The deep blue emitting nanoring has an appreciable quantum yield of 53% in toluene solvent. Host–guest analysis with C_{60} resulted in association with a binding constant of K_a = 9.95×10^4 M^{-1}. Owing to the ring size and D–A nature, the charge transport properties measured using the SCLC method resulted in nearly balanced hole and electron mobilities of 4.75×10^{-3} cm^2 V^{-1} s^{-1} and 1.87×10^{-3} cm^2 V^{-1} s^{-1}, respectively. Given the growing number of tested macrocycle-based organic electronic devices, we anticipate that the outcomes of this work will be beneficial and a leap-forward toward the development of macrocycles with superior charge carrier mobilities as well as the development of improved design principles.

Data availability

The data supporting this article have been included in the ESI.†

Conflicts of interest

The authors declare no conflicts of interest.

Notes and references

1 E. Nakamura, *et al.*, *J. Am. Chem. Soc.*, 2003, **125**, 2834–2835.
2 S. C. Kornmayer, *et al.*, *Chem. – Eur. J.*, 2009, **15**, 3380–3389.
3 (*a*) Q. Song, *et al.*, *J. Am. Chem. Soc.*, 2005, **127**, 13732–13737; (*b*) R. Jasti, *et al.*, *J. Am. Chem. Soc.*, 2008, **130**, 17646–17647; (*c*) W. Ying, *et al.*, *Acta Chim. Sin.*, 2023, **3**, 289–308; (*d*) Y. Wei, *et al.*, *Nat. Commun.*, 2024, **15**, 5438.
4 (*a*) Y. Segawa, *et al.*, *Org. Biomol. Chem.*, 2012, **10**, 5979–5984; (*b*) M. R. Golder and R. Jasti, *Acc. Chem. Res.*, 2015, **48**, 557–566.
5 T. J. Sisto, *et al.*, *J. Am. Chem. Soc.*, 2011, **40**, 15800–15802.
6 S. Q. Zhang, *et al.*, *ACS Nano*, 2017, **11**, 11701–11713.
7 C. Zhong, *et al.*, *Nanomaterials*, 2023, **13**, 1750.
8 B. G. Kim, *et al.*, *Adv. Funct. Mater.*, 2013, **23**, 439–445.
9 (*a*) C. Li, *et al.*, *J. Mater. Chem. C*, 2019, **7**, 3802–3810; (*b*) Y. Y. Liu, *et al.*, *Org. Lett.*, 2016, **2**, 172–175; (*c*) Q. Feng, *et al.*, *Adv. Funct. Mater.*, 2024, **34**, 2312622; (*d*) Y. Song, *et al.*, *J. Mater. Chem.*, 2007, **17**, 4483–4491.
10 T. C. Lovell, *et al.*, *Chem. Sci.*, 2019, **10**, 3786–3790.
11 C. Brouillac, *et al.*, *Adv. Opt. Mater.*, 2023, **11**, 2202191.
12 (*a*) L. H. Xie, *et al.*, *Org. Lett.*, 2006, **8**, 2787–2790; (*b*) H. X. Yuan, *et al.*, *Chin. J. Chem.*, 2021, **39**, 701–709.
13 (*a*) F. Lucas, *et al.*, *J. Mater. Chem. C*, 2022, **10**, 14000–14009; (*b*) F. Lucas, *et al.*, *Chem. – Eur. J.*, 2023, **41**, e202300934; (*c*) G. Zhang, *et al.*, *Mater. Chem. Front.*, 2017, **1**, 455–459.
14 E. R. Darzi, *et al.*, *J. Am. Chem. Soc.*, 2017, **8**, 3106–3114.
15 M. Hermann, *et al.*, *Angew. Chem., Int. Ed.*, 2021, **19**, 10680–10689.
16 C. E. Colwell, *et al.*, *Chem. Sci.*, 2020, **11**, 3923–3930.
17 T. Lu and F. Chen, *J. Comput. Chem.*, 2012, **5**, 580–592.
18 T. C. Lovell, *et al.*, *Angew. Chem., Int. Ed.*, 2020, **59**, 14363–14367.
19 S. Wang, *et al.*, *Chem. Commun.*, 2021, **72**, 9104–9107.
20 F. Lucas, *et al.*, *J. Am. Chem. Soc.*, 2021, **23**, 8804–8820.
21 S. Canola, *et al.*, *Phys. Chem. Chem. Phys.*, 2019, **4**, 2057–2068.
22 (*a*) Y. Zhang, *et al.*, *Adv. Funct. Mater.*, 2012, **22**, 97–105; (*b*) C. H. Chen, *et al.*, *Adv. Funct. Mater.*, 2009, **19**, 2661–2670.